MACHINE LEARNING IMPLEMENTATION IN RADIATIVE PROPERTIES PREDICTION FOR POROUS MEDIA

A Thesis

by

HYUN HEE KANG

Submitted to the Office of Graduate and Professional Studies of
Texas A&M University
in partial fulfillment of the requirements for the degree of

MASTER OF SCIENCE

Chair of Committee,	Shima Hajimirza
Committee Members,	Michael B. Pate
	Pavel V. Tsvetkov
Head of Department,	Andreas A. Polycarpou

December 2019

Major Subject: Mechanical Engineering

ABSTRACT

Predicting the radiative properties of porous media is highly important in many engineering applications (e.g. additive manufacturing). The radiative properties of packed beds highly depend on the geometry and configuration of the structures and the types of materials. The conventional method of computing these properties is through Monte Carlo ray tracing (MCRT) simulations which yield statistical approximations through random sampling of light beams traversing in the porous medium. In ray tracing, numerous light bundles are simulated traveling in random packed beds which are computationally structured via a discrete element model (DEM) of particle settlement simulation. The geometric complexity of porous medium poses computational challenges in both ray tracing and DEM simulations. As a result, MCRT calculations are extremely time-consuming and difficult to setup/program.

In this work, we demonstrate that machine learning (ML) techniques can be used to expedite the process of estimating the radiative properties of porous media. ML methods are used in two ways to this aim:

1) As predicative models to directly estimate the radiative properties as functions of the medium geometry and configuration parameters. Specifically, we use neural networks (NN) to predict the radiative properties of the media using supervised learning where the labeling data is collected using ray tracing. The out-sample prediction can be carried out without the execution of MCRT simulations. We demonstrate that the trained

NN models predict transmittivity of random packed beds with improved efficiency and preserved accuracy.

2) As characterization models to summarize and parameterize the statistical geometric properties of random beds which would lead to generation of surrogate penetration length distribution (PLD) functions. PLD is the distribution of probable extinction-free paths in the void between particles and is essential to MCRT simulations. Fast generation of surrogate PLDs essentially obviates the need for cumbersome DEM calculations thus leading to efficient approximate calculations of the radiative properties. ML techniques such as Gaussian Process (GP) modeling can be used for geometric characterization. Coupling ray tracing with the GP model transforms the randomness of the sphere packing into random light travel trajectories in the MCRT simulation. Without DEM simulations, The MCRT coupled with GP model accurately calculates radiative absorptivity.

ACKNOWLEDGEMENTS

I would like to thank my committee chair, Dr. Hajimirza, and my committee members, Dr. Pate, Dr. Tsvetkov, and my colleague, Mine Kaya, for their guidance and support throughout the course of this research.

Thanks also go to my friends and Prof. Yuval Doron for making my time at Texas A&M University a great experience. Finally, thanks to my parents and sister for their encouragement.

CONTRIBUTORS AND FUNDING SOURCES

Contributors

This work was supervised by a thesis committee consisting of Professor Shima Hajimirza and Professor Michael B. Pate of the Department of Mechanical Engineering and Professor Pavel V. Tsvetkov of the Department of Nuclear Engineering. All work conducted for the thesis was completed by the student independently.

Funding Sources

Graduate study was supported by a Graduate Assistantship of Teaching from the Department of Mechanical Engineering at Texas A&M University.

NOMENCLATURE

D	Particle diameter
e	Output error vector
E	regularized sum of squared error
f	transfer function
i	layer index
I	light intensity
ℓ	penetration length
L	bed height
M	number of network layers
n	unit surface normal vector.
N	number of folds
r	particle radius
R	number of neuron in hidden layer
S_n	normalized transmissivity
W	weight matrix
$\mathbf{v}$	vector form of the weight matrix
$\mathbf{y_0}$	input vector
$\mathbf{y_i}$	output of ith layer of neural network
β	extinction coefficient
ε	the surface emissivity of the particles

φ	Bayesian regularization parameters
λ	wavelength
p	percentile for penetration length
l	penetration length
α	absorptivity
θ	incident angle of ray
n	refractive index, $a+bi$
x_0	center coordinate of particle
x_1	start point of incident ray
x_2	end point of incident ray
u	directional cosine of incident ray
n	unit surface normal vector
γ, θ	directional cosines
h	basis function
σ^2	noise variance
θ	kernel parameter
k	covariance function
L	resubstitution loss
Cu	Copper
SS	Stainless steel
Ag	Silver
PMMA	Polymethyl methacrylate

Al2O3	Aluminium oxide
ZnO	Zinc oxide

TABLE OF CONTENTS

Page

ABSTRACT ii

ACKNOWLEDGEMENTS iv

CONTRIBUTORS AND FUNDING SOURCES v

NOMENCLATURE vi

TABLE OF CONTENTS ix

LIST OF FIGURES xi

LIST OF TABLES xii

CHAPTER I INTRODUCTION 1

1.1 Motivation 1
1.2 Problem 2
1.3 Literature review 4
1.4 Monte Carlo ray tracing 8
1.5 Neural networks 10
1.6 Gaussian process 14

CHAPTER II RADIATIVE PROPERTIES PREDICTION 15

2.1 Physical model 15
2.2 Penetration length probability distribution function 16
2.3 Monte Carlo ray tracing simulation for radiative properties 19
2.4 Neural network based surrogate modelling 22
2.5 Results and discussion 27

CHAPTER III GAUSSIAN PROCESS MODEL COUPLED WITH MCRT 33

3.1 Ray tracing simulation with polarization effect 34
3.2 Computational model of powder geometry 36
3.3 Machine learning based geometry abstraction 40
3.4 Modified ray tracing 41
3.5 Results and discussion 44

CHAPTER IV CONCLUSION 47

REFERENCES 49

LIST OF FIGURES

Page

Figure 1 Diagram of single hidden-layer neural network 11

Figure 2 Hyperbolic function 12

Figure 3 Monte Carlo simulation for penetration depth distribution 16

Figure 4 The closest particle selection for penetration length sampling 18

Figure 5 Penetration distance probability validation (modified from [6]) 19

Figure 6 Random particle center selection in ray tracing 20

Figure 7 Configuration of a two-layer neural network 23

Figure 8 Variation of training and validation error 25

Figure 9 MCRT validation and NN accuracy performance (modified from [3] & [6]) 28

Figure 10 Average MCRT computation time as a function of bed height (3 samples) 29

Figure 11 Average number of particle-light reflections 30

Figure 12 MCRT convergence study 32

Figure 13 Repeated random sampling of rays emitted to stainless steel powders 34

Figure 14 Sequential settling of individual rigid particles in MFIX 36

Figure 15 Penetration length probability density function 39

Figure 16 Modified ray tracing simulation 42

Figure 17 (a) Absorptivity comparison (b) Ray tracing performance 43

Figure 18 Performance of trained GP model 45

LIST OF TABLES

Page

Table 1 Upper and lower bounds for the training set 26

Table 2 Absorptivity calculations of AM materials (modified from [2] & [7]) 46

CHAPTER I

INTRODUCTION*

Thermal radiation is an important heat transfer mechanism in many engineering applications involving dispersed media operating at elevated temperatures. The following sections illustrate why thermal radiation in porous media is important and provide three relevant applications. We then define the main technical problem that this dissertation is trying to solve and lay out the approaches that will follow.

1.1 Motivation

Porous metals are widely used in aerospace applications ranging from aircraft to space instrument packages. Porous structures in metal can add unique characteristics to its original values. This uniqueness can allow long term service in filtration, flow control, or thermal management. The objective in these applications is the production of robust porous materials that function in a predictable and consistent manner over extensive periods of time in hostile environments. Among many others, one possible operation condition can be exposure to elevated temperatures ranging from 1600°F to 2000°F. In this case, the effect of thermal radiation should be investigated to optimize the design of porous metal components to achieve the best possible performance.

*Parts of this chapter's text is borrowed from the authors published paper, "A data driven artificial neural network model for predicting radiative properties of metallic packed beds," by Kang HH, Kaya M, and Hajimirza S, 2019. *Journal of Quantitative Spectroscopy and Radiative Transfer* 226, 66-72, Copyright 2019 by Elsevier. No permission is required.

Since many porous metals are manufactured via powder based sintering technology nowadays, the characterization of thermal radiation in porous media also serves a critical benefit to the optimization of 3D printing process. Additive manufacturing (AM) is a transformative approach to industrial production that increases digital flexibility and efficiency. AM includes technologies that grow three-dimensional objects one superfine layer at a time. Each successive layer bonds to the preceding layer of melted or selectively melted material. In selective laser sintering (SLS), laser is used to selectively fuse layering material. Multiple layering materials exist for SLS applications, such as metals, polymers, ceramics, composites, and even edibles. The study of laser interactions with these materials is of particular interest to selective laser sintering (SLS) development. The sintering process is characterized by a number of parameters, including the powder material, the layer thickness and porosity, the laser beam size and profile, and the laser scan speed. Reliable process modelling is very useful for determining the optimal parameters and anticipating possible problems in the build process.

1.2 Problem

Two major transport mechanisms in a randomly packed bed of spheres are conduction through the solid contact between spheres, and radiative transfer through the voids. However, these two processes can be decoupled effectively and considered separately [1]. The objective of this study is to develop a prediction model to characterize the radiative heat transfer process through the randomly packed bed of spheres.

The existence of multiple dependencies in this problem makes modelling complex. Firstly, the radiation in porous media largely depends on geometric properties of porous

media. Porous media can be made of particles or cavities with irregular shapes. These forms can be made naturally or artificially. For example, sands, sea bubbles, and animal bones are natural forms. Pebbles in PBR and AM layering powders are artificial forms. The size of elements can be different as well. For instance, elements in each PBR and AM powder bed have centi-meter and micro-meter scale, respectively. In addition, elements in porous media can have different size distribution and porosity. Along with bulk dimension of porous media, these geometric parameters are essential in radiative heat analysis because a heat interaction in porous media changes depending on which phases radiation interacts with.

Secondly, Radiative conductivity (thermal conductivity due to photon transport) of porous media can change significantly with temperature. Also, if temperature gradient is large inside the pores. The radiative properties prediction becomes difficult.

Thirdly, the optical properties of porous media elements change with material and radiation wavelength. The surface of an element in porous media shows a distinct spectral dependence to radiation. For simplicity, opaque, semitransparent, or transparent surface assumption are widely used in many studies. An opaque surface does not allow transmission and absorbs a given fraction of the thermal radiation a blackbody surface would absorb. The radiation on an opaque surface is independent of radiation wavelength. Meanwhile, the radiation on semitransparent or transparent surface partially transmits through the surface and experiences refractions. Instead of the three surface assumptions above, the Fresnel equation can be used to account for wavelength, angular, and polarization dependency [2]. Radiative reflection on a particle surface can be interpreted

in different ways as well. Specular (mirror like) or diffuse reflection can be assumed. Otherwise, more complex consideration such as anisotropic scattering distributions or directional surface properties should be considered. In case that particle size or interspacing are too small compared to radiation wavelength, a near field effect should be considered in radiative heat analysis. If optical thickness of porous media is too thin, a diffuse model is not valid because absorption is highly nonuniform [3]. If the thickness is too thick, accurate calculation is difficult because of weak intensity of transmission through porous media [4].

Lastly, other heat transfer phenomenon and mass transfer can occur simultaneously. For instance, the pore structure of powders changes drastically in actual laser sintering process. Particles' shapes and size distribution also changes due to melting and rearrangement. There could also be a phase change such as metal evaporation. For this study, steady packed bed models with perfect sphere particles is used and temperature independence is assumed.

1.3 Literature review

The problem of thermal radiation in dispersed (porous) media has been studied for decades. Most of the early studies (e.g. [5], [6],[7]) experimentally determined the effective radiative properties of isothermal packed beds of semitransparent and opaque particles. The absorptance of material is the ratio of the absorbed radiation to the incident radiation, and the reflectance is the ratio of reflected radiation to the incident radiation. In the experiments, the radiation reflected by the powder is generally measured with photo-receiver and integrating sphere. Then absorptance is calculated by subtracting reflectance

from unity. In general, the absorptance depends on the laser wavelength, material properties, geometric properties, ambient gas, temperature, etc.

Due to difficulties in direct measurement of the radiative properties, analytical or numerical approaches are commonly used to approximate the radiative properties. When the dispersed media is statistically homogeneous and isotropic, the classical radiative transfer equation (RTE) is used, while for poly-dispersed or anisotropic particles generalized RTE is suggested [8]. RTE is generally solved by means of Monte Carlo Ray Tracing (MCRT) simulations [4], [9], [10] since there is no explicit solution for most problems. Depending on the problem, different physical phenomena are involved in the MCRT framework. For example, the interface of the porous medium can be treated as opaque [10] or semitransparent [11] depending on the material type, which introduces refraction, internal scattering, absorption, and possibly emission. Furthermore, the interference effect among scattered waves (i.e. dependent scattering) is accounted in cases where particles are closely packed or relatively small compared to wavelength of radiation source [12], [13]. The prediction of absorption for layering materials used in AM is a useful application of ray tracing approaches. An initial ray tracing model for this application is developed by Wang et al [14]. Later, the angular and polarization dependence of the absorption of incident rays is added to the model [2]. Although numerical calculation of absorption through ray tracing is generally accurate, the computation can be exhaustive if the background geometry is too complex to model or perform ray tracing.

Geometric characteristics of porous medium change the scheme of heat transfer and accurate realization of porous medium is critical in MCRT simulation. The implementation of MCRT requires a numerical procedure for simulated generation of random porous media platform, which is called the packing algorithm. Various types of packing algorithm have been recommended and used (see e.g. [15], [16]). Some recent works such as that of Tancrez and Taine [17] have recommended using alternative statistical methodologies based on the Monte Carlo scheme to determine the radiative properties of computer generated structures [17], [18] and real porous media obtained by tomography [19]–[21]. This statistical method was generalized by Chahlafi et. al. [22] in the work of radiative heat transfer modelling for statistically anisotropic porous media with non-Beerian homogenized phases.

MCRT simulations require intense computational resources. The source of high computational cost is the iterative simulation process on dispersed media with complex geometry and/or large numbers of particles. This computational cost can hinder an exhaustive procedure to solve an inverse problem in which a specific geometry is sought for a given radiative property or to control radiative power such as SLS. In order to overcome the computational barrier, several researchers have suggested using alternative analytical formulations. For instance, Randrianalisoa and Baillis have done rigorous work on analytical formulation of radiative properties of statistically isotropic and homogeneous dispersed media [23]. Dombrovsky and Baillis introduced user-friendly and easy to implement approaches to apply analytical solutions to practical engineering problems [24]. Nevertheless, the scopes of the solutions these methods offer is limited. MCRT

remains a widely used method for modeling thermal radiation in dispersed media, as it provides accurate estimations in spite of intense simulation times [25].

The prediction of absorption for powders used in AM is a useful application of this approach. An initial ray tracing model for this application was developed by Wang et al [14]. Later, the angular and polarization dependence of the absorption of incident rays was added to the model [2]. Although numerical calculation of absorption through ray tracing is generally accurate, the computation can be exhaustive if the background geometry is too complex to model or perform ray tracing.

1.4 Monte Carlo ray tracing

The Monte Carlo method is a numerical technique based on the statistical characteristics of physical processes. At first, this approach was developed to analyze the potential behavior of nuclear weapons as a replacement of difficult experiments and inaccurate approximation models available at that time [26]. Sufficient random sampling of individual neutron behavior in simulation and analyzing observed behaviors of neutrons allowed approximation of the average behavior of the weapon.

The Monte Carlo method is an effective solution to radiative heat transfer studies. The radiative heat transfer equations (RTE) are complex and difficult to solve. If complex physical effects such as spatial variation of properties are involved in radiative transfer, deterministic mathematical models become inapplicable. In addition, various degrees of approximation is inevitable to solve the RTE and exact analytical solutions to RTE are not available except for simplified choices of geometries. Meanwhile, the Monte Carlo method can account for all important effects in a radiative transfer simulation without incorporating a degree of approximation.

In ray tracing, two important rules are all rays travelling in a system must obey the laws governing radiation and every event must be independent of the preceding events. Random porous media geometry or radiation trajectory can ensure the event independence in ray tracing. This randomization can be done by using a uniform set of random numbers in the range between 0 and 1. If the probability of any event is known, a random choices from this distribution can be made by applying Eq. (1).

$$R = \int_{\xi^*=-\infty}^{\xi} dP(\xi^*). \qquad (1)$$

The typical characteristics of Monte Carlo analysis are observed in ray tracing as well. First, the approximation becomes more accurate as more samples are included in the simulation. The second characteristic is that accuracy tends to depend on the square root of the increase in sample packet number. For example, running four times the number of packets in simulation will reduce uncertainty by one-half.

Using the Monte Carlo method, physical relations that are repeated replace a degree of mathematical sophistication. As a result, complicated radiative heat transfer problems can be easily programmed. However, ray tracing may require lengthy computational time depending on the complexity of the problems.

1.5 Neural networks

A neural network (NN) models desired output as a nonlinear function of linear combinations extracted from input. The operation of forming nonlinear functions of linear combinations generates a surprisingly large class of models. Thus, a large class of nonlinear statistical models and learning methods are in NN category. This generality has drawbacks. Multi-faceted interconnections between input and output make interpretation of the fitted model difficult. A NN model can perform well for prediction but it is hard to come up with comprehensible model for the data.

In this study, the single hidden layer back-propagation network is covered. A NN is a two-stage regression or classification model, typically represented as Figure 1. Derived features Z_m are created from linear combinations of the inputs, and then the target Y_k is modeled as a function of linear combinations of the Z_m. Hidden and output layers can have bias unit which captures the intercepts α_{0m} and β_{0k} in Eq (2).

$$\begin{aligned} Z_m &= \sigma(\alpha_{0m} + \alpha_m^T X), m = 1, \dots, M, \\ T_k &= \beta_{0k} + \beta_k^T Z, k = 1, \dots, K, \\ f_k(X) &= g_k(T), k = 1, \dots, K, \end{aligned} \qquad (2)$$

The activation function σ checks the Y value produced by a neuron and decide whether outside connections should consider this neuron as activated or not. The hyperbolic function in Figure 2 is a popular activation function because of many benefits. First, the hyperbolic function is nonlinear in nature and the combinations of this function

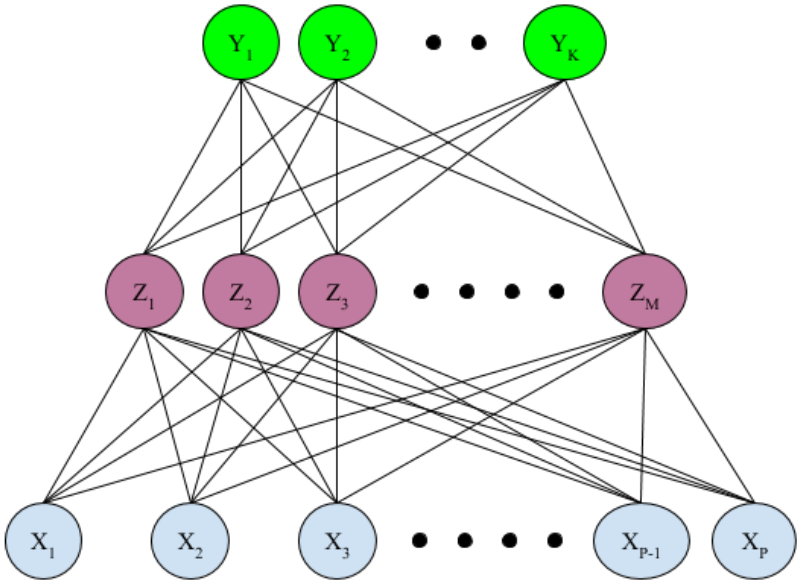

Figure 1 Diagram of single hidden-layer neural network

are also nonlinear. This characteristic of the hyperbolic function allows stacked layers in a NN architecture. Another advantage of this activation function is that the output of the activation function is in range from 0 to 1. Thus, activations bound in a range and do not bound off to infinity. In addition, the hyperbolic function enables an analog activation with smooth gradient unlike binary activations. However, the *Y* values tend to respond very less to changes in *X* towards either end of the hyperbolic function. The gradient at the region is small and it gives rise to a problem of "vanishing gradients". When the activations reach near the horizontal part of the curve, gradient is small or vanished. Due to vanished gradient, the network refuses to learn further or is drastically slow.

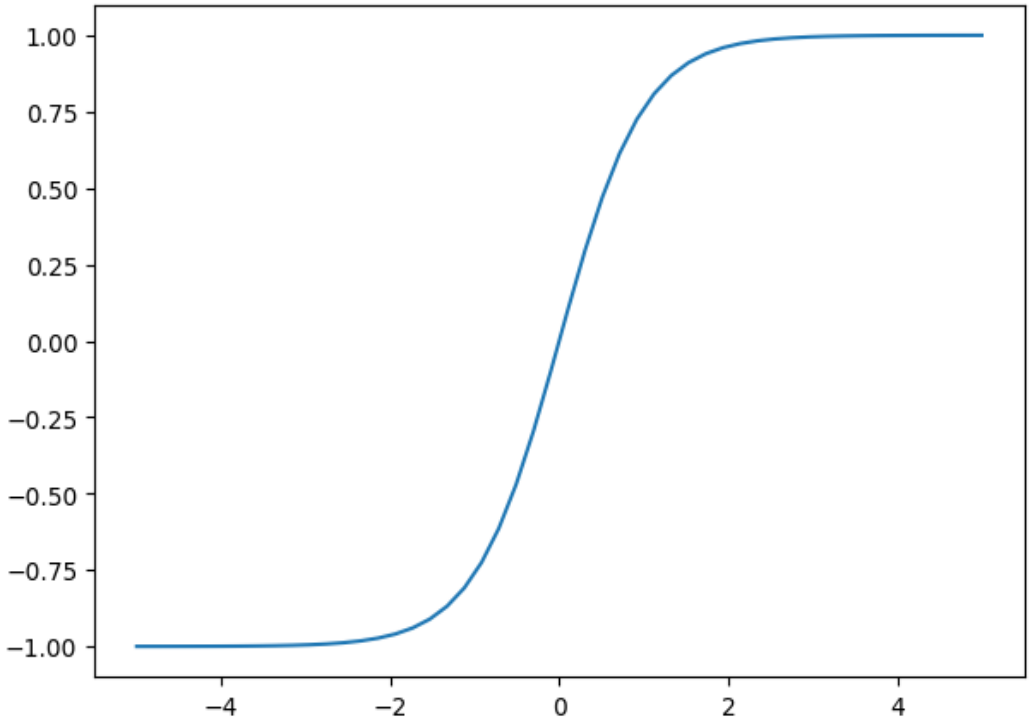

Figure 2 Hyperbolic function

The hidden units in the middle of the network are not directly observed but compute the derived features Z_m. If Z_m is considered as a basis expansion of inputs X, the neural network is just a standard linear model. Various techniques are available to enhance over the basis expansion.

One of important process in NN modelling is fitting neural networks. The neural network model is composed of unknown parameters, often called weights, and values for them should be optimized so that the model fit the training data well. For regression, sum-of-squared errors is used as the measure of fit (error function).

$$R(\theta) = \sum_{k=1}^{K}\sum_{i=1}^{N}(y_{ik} - f_k(x_i))^2 \qquad (3)$$

Typically the global minimizer of $R(\theta)$ is not desired due to overfitting. Instead some regularization is required through either using penalty term or indirect early stopping. The gradient descent is commonly used to minimize $R(\theta)$.

Using errors from the current model at the output and hidden layer units, the following back-propagation equations can be solved with two-pass algorithm.

$$s_{mi} = \sigma'(\alpha_m^T x_i)\sum_{k=1}^{K}\beta_{km}\delta_{ki} \qquad (4)$$

The forward pass computes the predicted values $\widehat{f_k}(x_i)$ by applying Eq (2) with the current weights. The backward pass back-propagates the computed errors δ_{ki} via Eq (4) and calculate the errors s_{mi}. Next, the gradients are updated with computed errors. This two-pass procedure is famously known as back-propagation.

The back-propagation process is simple and happens locally. However, back-propagation is not preferred in many times due to its slow process. Second-order techniques such as Newton's method are not attractive as well due to the same reason. Instead, conjugate gradients and variable metric methods can be used for fitting. These allow faster convergence without explicit computation of the second derivative matrix.

1.6 Gaussian process

A Gaussian process (GP) is a generalization of the Gaussian probability distribution. While a probability distribution describes random variables which are scalars or vectors (for multivariate distributions), a stochastic process governs the properties of functions. Assuming a function as a very long vector, each entry in the vector specifies the function value f(x) at a particular input x. These infinite dimensional objects in the vector impose computational problems. Using the properties of the function only at a finite number of points, the inference in the Gaussian process provides the same answer as if infinite points are taken all into account. One of the main attractions of the Gaussian process framework is precisely that it unites a sophisticated and consistent view with computational tractability.

A GP model is kernel-based probabilistic model [27]. A GP can predict the value of a response variable y_{new}, given the new input vector x_{new}, and the training data. A linear regression model is of form:

$$y = x^T\beta + \epsilon \tag{5}$$

Where $\epsilon \sim N(0, \sigma^2)$. The error variance σ^2 and the coefficients β are estimated from the data. The cores of GP model are latent variables $f(x_i)$ from GP and explicit basis functions. Latent variables are inferred from other observed variables. The covariance function of the latent variables explains the smoothness of the response and basis functions map original feature space into new feature space. Based on data observations, this basis function condition the GP prior and produce the GP posterior.

CHAPTER II

RADIATIVE PROPERTIES PREDICTION*

This chapter demonstrates that machine learning methods can be reliably used to predict radiative properties of dispersed media, i.e. packed beds, as a function of packed bed geometry and material properties. The computationally expensive Monte Carlo ray tracing (MCRT) method, which is widely used in this context, is replaced by Neural Networks (NN). We demonstrate that the data-driven surrogate prediction works accurately and generally. The results of both MCRT and NN models agree well with each other and with previously measured literature results. We also measure the uncertainty of the NN results using statistical methods. It is recommended that the developed model be used for efficient inverse problems and optimizations in relevant future work.

2.1 Physical model

In this study, a physical system with monodispersed spherical particles randomly packed in a semi-infinite bed is considered. The particle packing procedure is modeled via the open source Discrete Element Method (DEM) particle simulation software called MFix. This simulation provides the location of the randomly packed particles in the bed to be used in MCRT simulations. In this study, we first compute the penetration length distribution via MCRT simulation, and then use this distribution in additional MCRT

*Reprinted with permission from "A data driven artificial neural network model for predicting radiative properties of metallic packed beds." by Kang HH (the thesis author), Kaya M, and Hajimirza S, 2019. *Journal of Quantitative Spectroscopy and Radiative Transfer* 226, 66-72, Copyright 2019 by Elsevier. No permission is required.

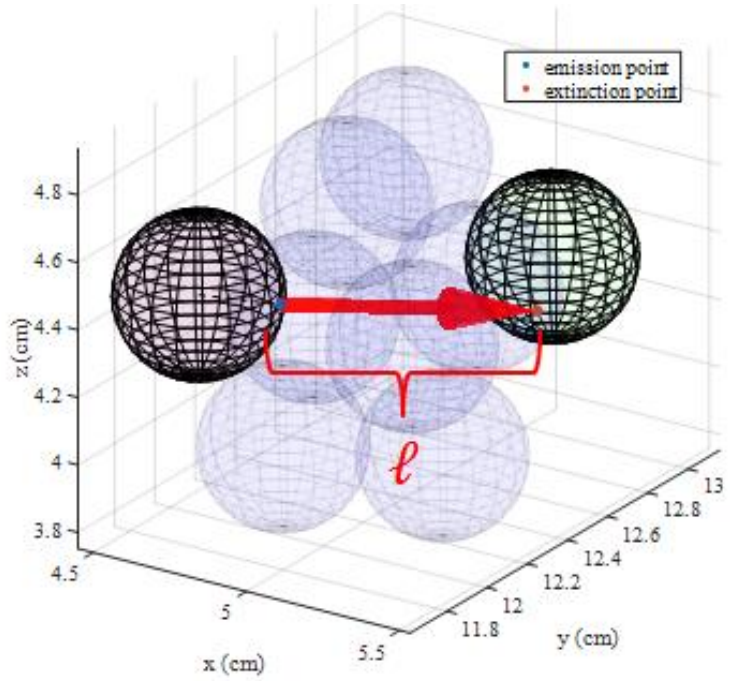

Figure 3 Monte Carlo simulation for penetration depth distribution

simulations to calculate other radiative properties of the media. This approach provides additional computational efficiency since the complete set of particle location information is not stored during simulations [28].

2.2 Penetration length probability distribution function

The penetration distance (ℓ) in a dispersed medium is defined as the distance that a light bundle travels in the void before hitting a particle surface. Pre-calculation of the probability distribution function of ℓ increases computational efficiency as described in the next section. The characterization of the probability function requires extinction coefficient (β) approximation based on the Beer-Lambert Law [29]:

$$I_l = I_o \exp\left(-\int_0^{\ell} \beta \, d\ell\right). \quad (6)$$

where I_o is the initial amount of energy of the light bundle and I_l is the amount of energy that remains in the light bundle after the light travels a distance ℓ. The distributions of β and ℓ are equivalent. More details can be found in the reference [28].

The penetration depth ℓ calculation starts with randomly selecting a base sphere and a random (emission) point on its surface. Then a light bundle is sent through a random direction. This light bundle is traced from random emission points to extinction points where it loses energy due to interaction with a particle (Figure 3). Spheres on the ray projection are found by evaluating perpendicular distances between the projection of ray and all sphere centers, then selecting the one closest to the emitting sphere to calculate a penetration length as shown in Figure 4. This procedure is repeated 5,000 times to achieve the penetration depth distribution. It is also possible to express the probability distribution as the cumulated probability distribution using standard statistical relations. The resulting probability function and comparison with the literature [28] are shown in Figure 5. ℓ/r is the ratio of the penetration distance to particle radius. A light bundle is most likely to travel to a distance of approximately half of a sphere radius, and only 1% of the overall light bundles can travel more than 4.4 times the sphere radius. It is worth mentioning that ray tracing methods are valid only when geometric optics laws are applicable, which is the

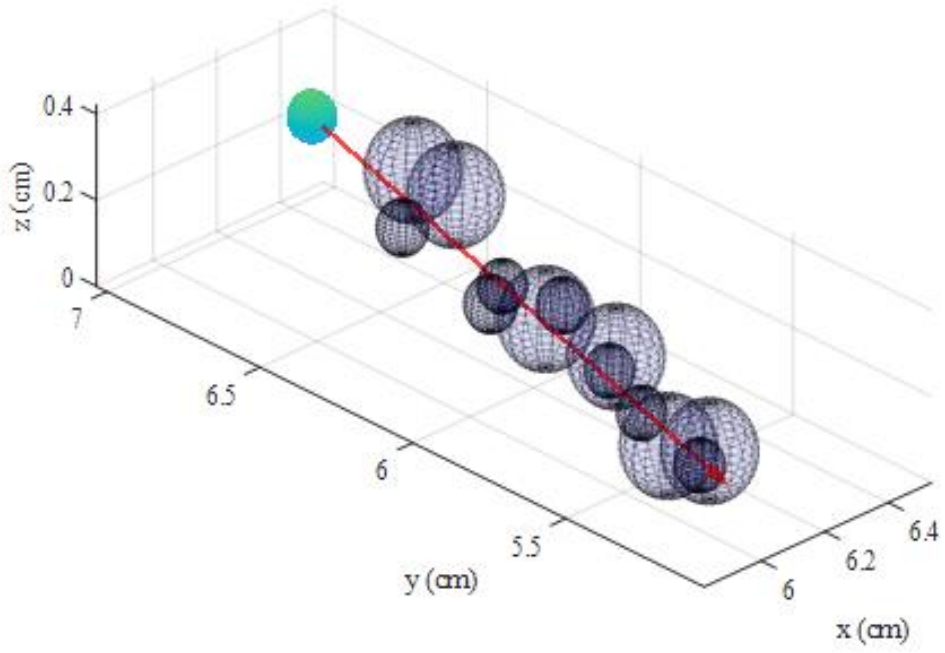

Figure 4 The closest particle selection for penetration length sampling

case when the particle dimensions are much larger than the radiation wavelength ($\pi D/\lambda \gg 1$) [30]. In the present study, a packed bed of mono-sized spherical particles with a diameter and average packing clearance much larger than operating wavelength is considered. Additionally, the particles and the void are assumed to be opaque and transparent, respectively.

2.3 Monte Carlo ray tracing simulation for radiative properties

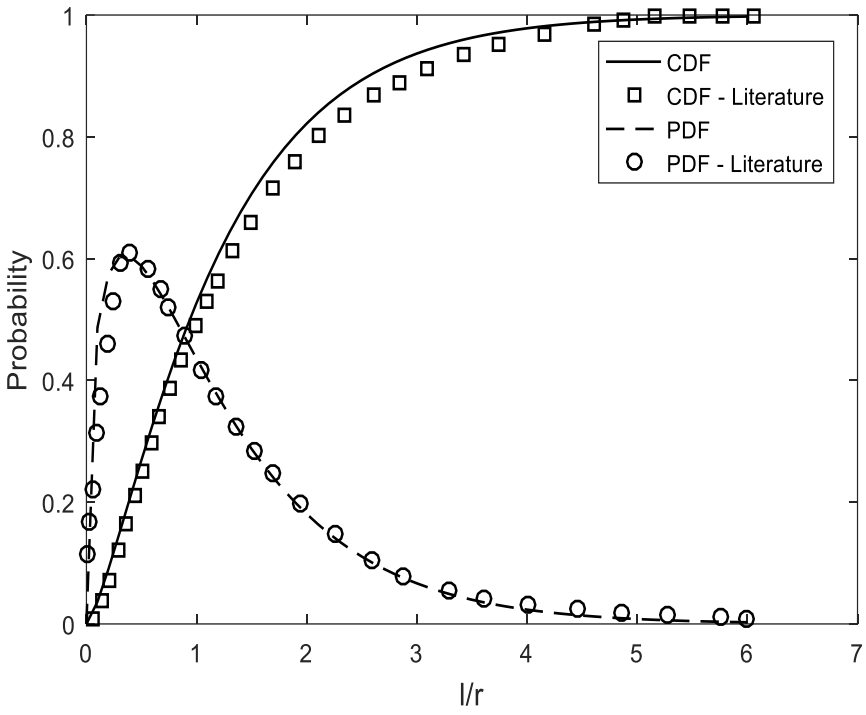

Figure 5 Penetration distance probability validation (modified from [6])

The MCRT simulation statistically approximates the transmissivity of a random packed bed characterized by a particle radius, height of packed bed, and surface emissivity. In simulation, the random packed bed structure is gradually constructed as a light bundle travels through the bed using penetration depth distribution (*i.e.* the simulation does not preset the structure before light travel simulation). The light bundle transmits through vacuum void in the bed and experiences absorption and scattering due to metal particles. This simultaneous process of structure formation and ray tracing reduces the

computational cost significantly. With sufficient iterations, the transmissivity of the bed

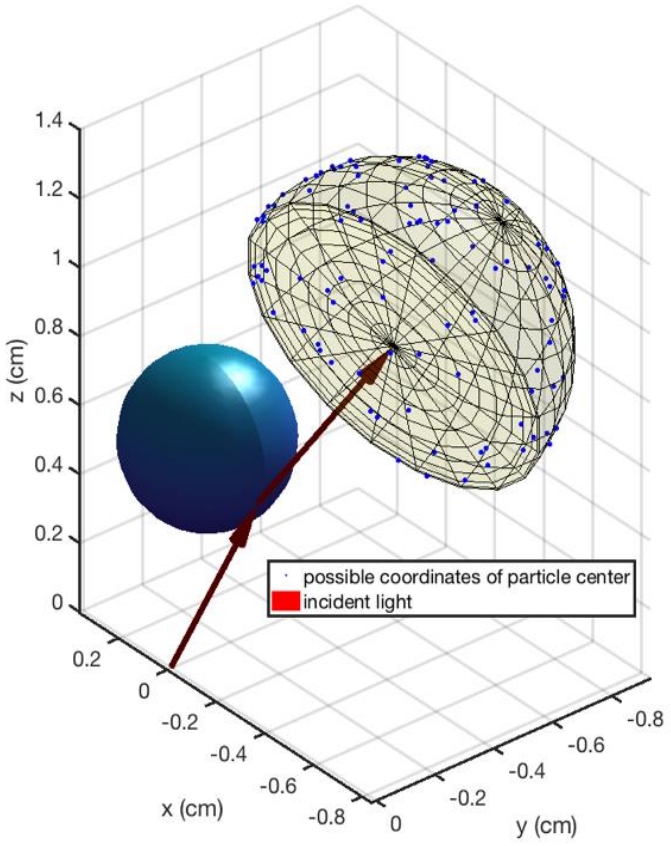

Figure 6 Random particle center selection in ray tracing

can be statistically determined for given input parameters.

An iteration loop starts with emitting a light bundle from the origin. The location of a sphere hit by the light bundle is determined by a randomized approach which includes a random penetration distance and random direction cosines. A penetration distance drawn randomly from the cumulative density function in Figure 5 gives the magnitude of the

direction vector, and the directional cosines are calculated from the random angles, R_γ γ and R_θθ, as follows:

$$\gamma = \sin^{-1}\left(R_\gamma^{0.5}\right) \tag{7}$$

$$\theta = 2\pi R_\theta. \tag{8}$$

Once the collision point is determined based on the emission point and the direction vector, the center coordinates of the sphere is chosen randomly from Eq. (7). and Eq. (8). The possible centers form a hemisphere pointing in the direction of incident light from the collision point (see Figure 6). The impenetration constraint between spheres is considered to prevent overlapping. Applying gray surface assumption, a fraction of light bundle energy, namely $(1-\epsilon)E$, is attenuated at a collision point. E represents the light bundle energy. The light bundle is reflected specularly after collision. A reflection angle is calculated from the following Eq. (9).

$$u_j' = u_j - 2n_j \sum_{k=1}^{3} n_k u_k\,, \quad j = 1,2,3 \tag{9}$$

where u_j is the direction cosine of the incident ray and n_j is the component of the unit surface normal vector. With newly calculated directional cosines, the light bundle propagates to a next position determined by a new randomly drawn penetration distance. This process continues until one of three conditions is met: (1) light scatters back below the reference origin, (2) it passes over the top boundary of the packed bed, or (3) it loses its entire energy within the bed. The normalized transmission is approximated by dividing

the total energy of bundles passed through the packed bed by the total energy of light bundles emitted in the bed.

2.4 Neural network based surrogate modelling

Surrogate modeling has been proposed to replace simulations which demand high computational costs with faster approximate alternatives. When the objective is to design and optimize a structure, it is required to solve an inverse problem to find the desired input parameters. That in turn requires many number of successive simulations to be carried out, thus the computation cost is significantly high. A surrogate model can decrease the computational cost by approximating the complicated relationship between inputs and outputs as a response surface. This surface is a predetermined function or distribution which maps the input space to the output. There are many different surrogate modeling approaches available in the literature. The most common ones are polynomial regression, Neural Networks (NN) and Gaussian Process (GP). Among the many available options, NN has the ability to approximate almost every function with arbitrary degrees of nonlinearity and high generalization capability [31]. A brief explanation of NN is presented in the next section.

NN is a machine learning tool inspired from the neuron connections in the human brain. It transfers information (the input vector) to output through a series of functional

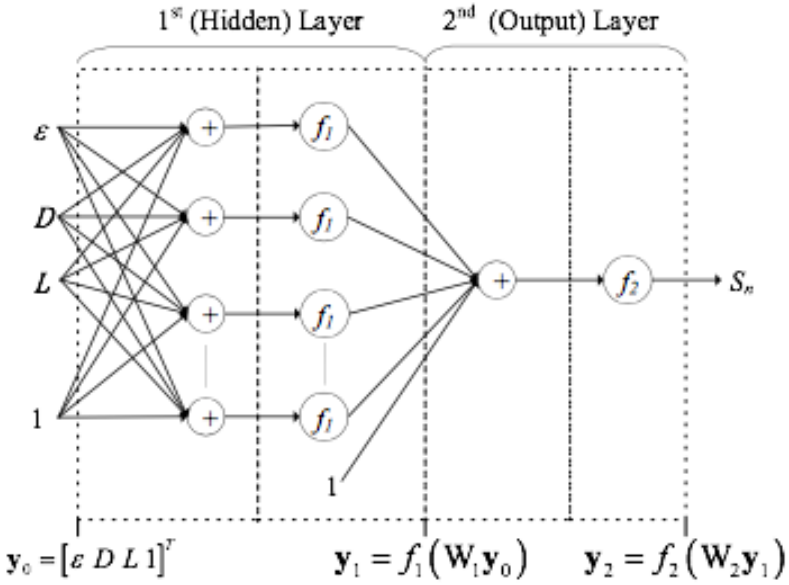

Figure 7 Configuration of a two-layer neural network

operations. These operations are performed in so-called neurons, which are connected to each other in parallel and in series. The parallel connected neurons constitute a layer of NN, while layers are connected in series. In general, two layers are enough for accurate and general prediction of most functions [32]. In a two-layer configuration (see Figure 7), the last layer is called the output layer, in which the number of neurons must be equal to the number of function outputs. The other layer is called the hidden layer. The number of neurons in the hidden layer is determined by NN training and construction, which will be explained in the sequel. The output of NN is calculated from

$$\mathbf{y_i} = f_i(W_i \mathbf{y_{i-1}}), \forall 1 \leq i \leq M$$

$$\mathbf{y_0} = [\varepsilon, D, L, 1]^{\mathbf{T}}, \quad (10)$$

where $\mathbf{y}_0$ is the input vector, M is the number of network layers, i is the layer index, W is the coefficient matrix determined as a result of NN training, and $\mathbf{y_i}$ and f_i are the output and the transfer function of the i^{th} layer, respectively. Variations of Sigmoid function are the most commonly used transfer functions. In the present study, tan-sigmoid is used in both layers as the transfer function. NN is trained in order to minimize the regularized sum of squared error:

$$E(\mathbf{v}) = \varphi_1 \mathbf{e^T e} + \varphi_2 \mathbf{v^T v}, \quad (11)$$

where $\mathbf{e} = \mathbf{t} - \mathbf{y_M}$ is the output error vector and $\mathbf{v}$ is the vector form of the weight matrix W. The term $\mathbf{e^T e}$ controls the quality of the fit and the $\mathbf{v^T v}$ term is added to the cost function in order to obtain a smoother function response thus avoiding overfitting. φ_1 and φ_2 are the Bayesian regularization parameters set iteratively [31]. The details of backpropagation NN training can be found in [31], [33]. In the present study, the input consists of the physical parameters, namely the surface emissivity of the particles ϵ, particles diameter D and bed height L. A constant bias is also always included in the input vector as scalar 1 as well as in the hidden layer during training. Validation set refers to the additional set of input-output pairs which provide intuition about the future (out-sample) performance of the NN. During training, $E_{val}(\mathbf{v})$ is recorded at every iteration, and once E_{val} starts increasing, training is terminated. The number of neurons in the hidden layer is determined by a similar procedure. Training is repeated for different

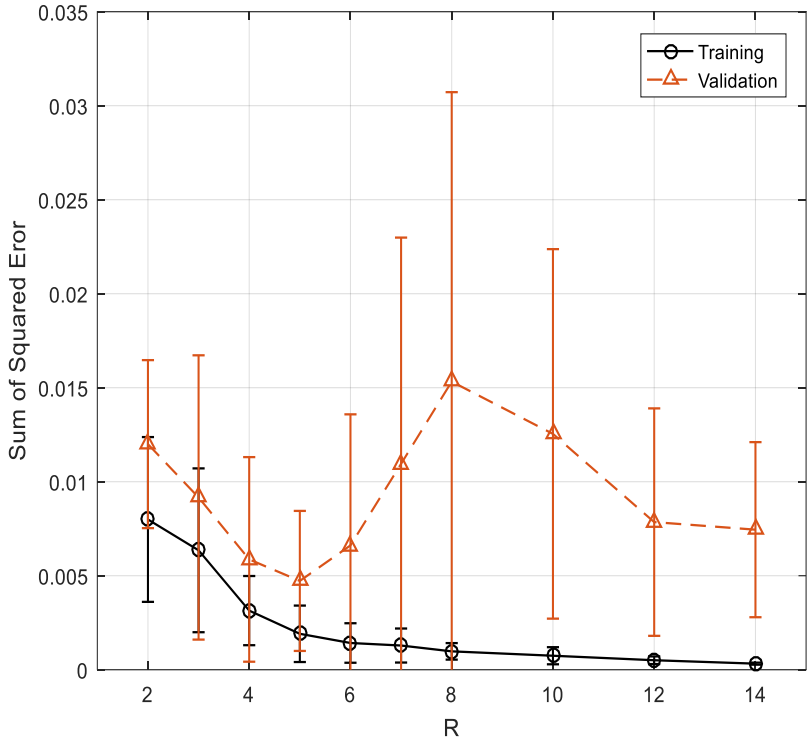

Figure 8 Variation of training and validation error

numbers of neurons, and the least number of neurons providing the smallest validation error is selected [34]. Among the available options [35], cross validation (CV) obtains an unbiased approximation and is a common method of choice. In CV, the data is divided into N folds, and training is done N times by using (N-1) folds in training, and 1-fold in validation.

3-*R*-1 NN model of transmitted power of a packed bed is trained following the procedure explained in the previous section. Here, 3 refers to the number of inputs, *R* is the number of neurons in the hidden layer and 1 represents the number of outputs. Inputs

for the training set are generated uniformly within the ranges presented in Table 1 and the target outputs are obtained by performing MCRT simulations for the corresponding inputs. It is important to note that the ratio of the bed height to particle diameter (D/L) is set to not exceed 12 in input set generation. This restriction excludes infinitesimally small transmission output in training data, and eventually prevents undesirable uncertainty in NN models.

Table 1 Upper and lower bounds for the training set

Parameter	ε	D [cm]	L [cm]
Lower Bound	0	0	0
Upper Bound	1	3	36

In general, there is a trade-off between the generalization of the regression model and the number of required computations in surrogate modeling. To increase the accuracy and reliability, increasing the number of data seems to be the best option. However, data acquisition computational time also increases with more data, which is a drawback. Therefore, an adaptive sampling procedure is employed during the training, which calls for the sequential increase of sampled data to be used in training. As a result, a total of 800 data is obtained and the data is divided into 4 folds where training with CV can be done. The sufficient number of neurons in the hidden layer (R) is determined such that the smallest resulting network with smallest validation error is obtained, as demonstrated in

Figure 8. The corresponding sum of squared errors for each value of R is plotted in error bar format (mean and standard deviation) for all 4 training instances.

2.5 Results and discussion

In this section, the MCRT solver for predicting transmissivity of packed beds is validated with previous MCRT models and experimental studies. Accuracy and computational efficiency of NN models are then investigated. Finally, uncertainties in both MCRT and NN model are analyzed to provide directions in further development.

Normalized transmission is calculated with respect to bed height, given surface emissivity of 0.4 and sphere diameter of 0.476 cm for the sake of validation and comparison with previously existing literature results. A total of 5000 energy bundles are emitted in MCRT. Figure 9a shows the comparison of transmission values obtained from the current MCRT model with those of previous studies. The output of NN model is compared with results of MCRT simulation in order to validate the performance of trained neural networks in Figure 9b. 30 different NN models were generated to quantify the uncertainty using the same number of neurons in the hidden layer ($R = 5$) and data set. The mean values align well with MCRT simulation output, but extra work is required to reduce variances between different networks. Active learning is one possible way to can improve generalization in neural network training by pointing out good examples from training data sets [36]. Another possible solution is to introduce uncertainty estimators in optimization cycles [37]. The performances of both MCRT and NN models were plotted with logarithmic scale on the y-axis which makes interpretation of the uncertainties more difficult. The alignment in each plot suggests two models have close power law relationships. However, this

agreement is necessary but not sufficient to prove both power law relationships because it cannot rule out alternate functional forms [38]. In this regard, more rigorous uncertainty analysis is required and new models coming after future accuracy improvements should be evaluated in careful manner.

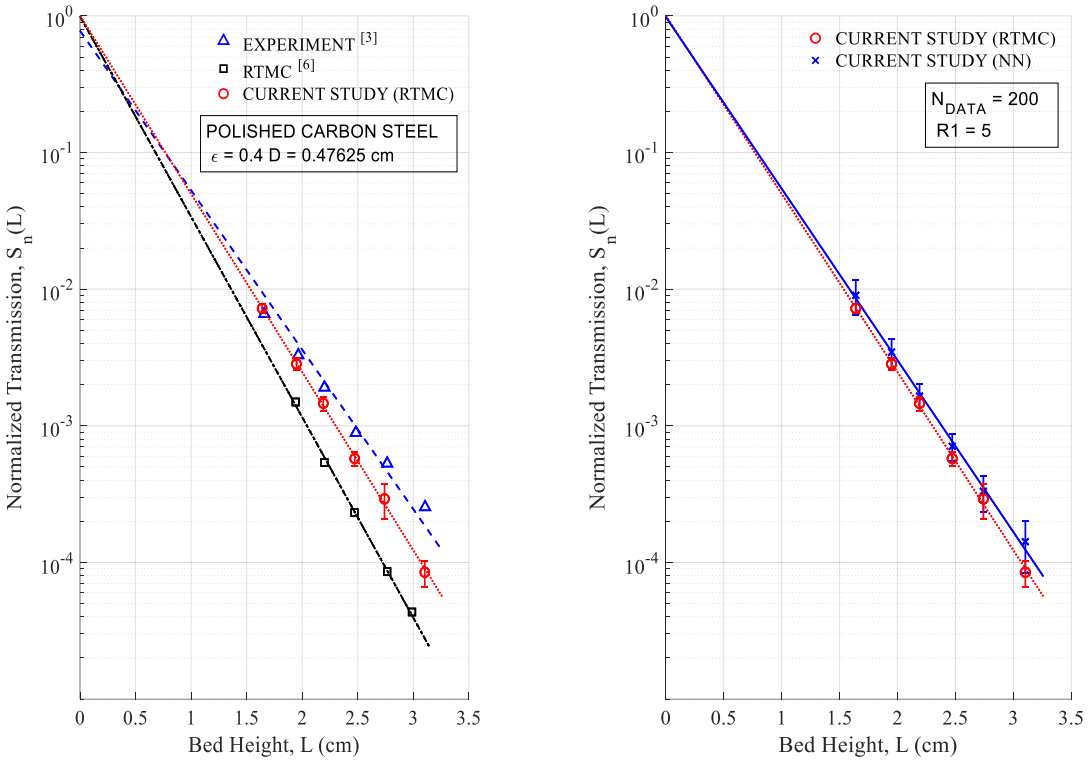

(a) **(b)**

Figure 9 MCRT validation and NN accuracy performance (modified from [3] & [6])

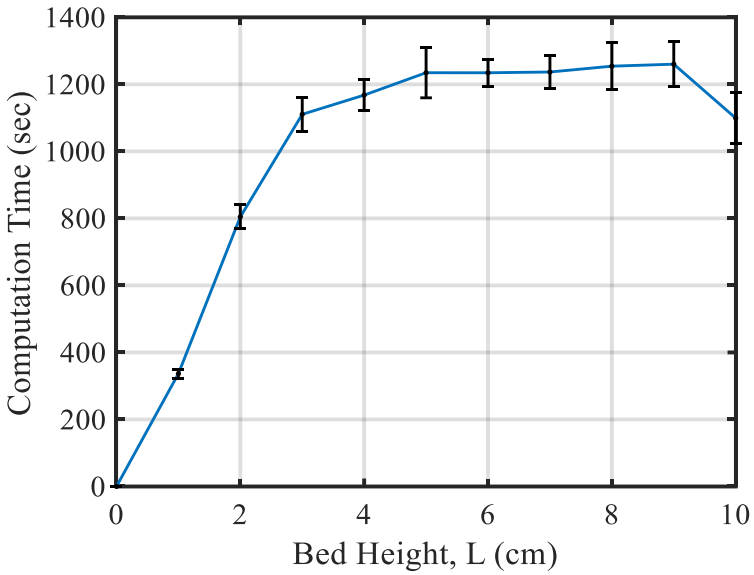

Figure 10 Average MCRT computation time as a function of bed height (3 samples)

The most expensive process of ray tracing simulation is tracing the successive light-particle interactions. In other words, the CPU time of MCRT simulation largely depends on how many collisions a ray makes with particles in each travel. A ray is more likely to travel longer in packed beds with taller heights. Indeed, Figure 10 shows the increase in computation time with respect to bed height, and Figure 11 supports the dependency of CPU time to number of light-particle interactions in simulations. However, the computation time appears to stop increasing at some point. As the depth of bed increases, the number of rays transmitted through a packed bed decreases. Instead, more energy is either scattered or absorbed by particles. Thus, the difference in the transmission output is no longer statistically significant after that critical point. Having said that, the

determination of this convergence point can be helpful to efficiently obtain training sets sufficient data points and partially reduce errors in trained networks.

The processing time required to predict transmission values of 100 uniformly distributed random input parameters is generally less than 24 hours. In neural network training, the search time of weight and bias for neurons in a hidden layer varies with

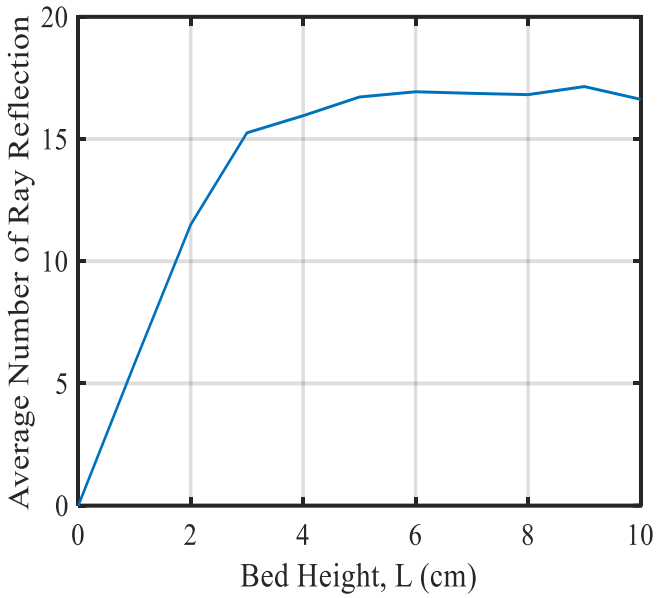

Figure 11 Average number of particle-light reflections

network structure, training data set, target error tolerance, step size, number of steps, randomness in search process, computing power, etc. The trainings in this study are processed with 5 neurons in a hidden layer, 200 training data, and 500 search iterations. A prediction is made by the trained surrogate model in around 10 seconds. The specification of computer used for training can be found at the end of paper. It is important to note that the cumulative probability density function is formulated in the current study

to statistically determine penetration distance in simulations. This function is implemented in the ray tracing algorithm to reduce computational cost of building the random geometry using DEM. If multiple random packed bed structures are used instead of the probability model, the time required to generate these structures should also be considered. Although the trained NN model makes accurate approximations with excellent computational efficiency, the demanding works involved in obtaining training data should not be omitted. Consequently, efficient surrogate modelling is essential to make machine learning approaches more viable for practical applications.

The law of large numbers is the basis of Monte Carlo method and it is an essential tool to determine how many samples are needed for reliable Monte Carlo results. The number of lights in MCRT simulation should be enough to guarantee stable long-term results for the averages of total energy transmitted through packed beds. For this reason, the effect of the number of rays on transmission output is investigated by running MCRT simulations with 10 different iteration numbers at three bed depths. The results of the convergence study in Figure 12 concludes that 5000 number of rays is enough in the simulation at all tested depths. The mathematical formulation of direct MCRT is relatively simple. The method can handle wide ranges of solid materials and complex geometries of dispersed media. However, the discrepancy between MCRT simulations and experiment emphasizes the importance of developing more realistic tools. The deviation between MCRT and experiment results of [39] can occur due to a variety of reasons such as

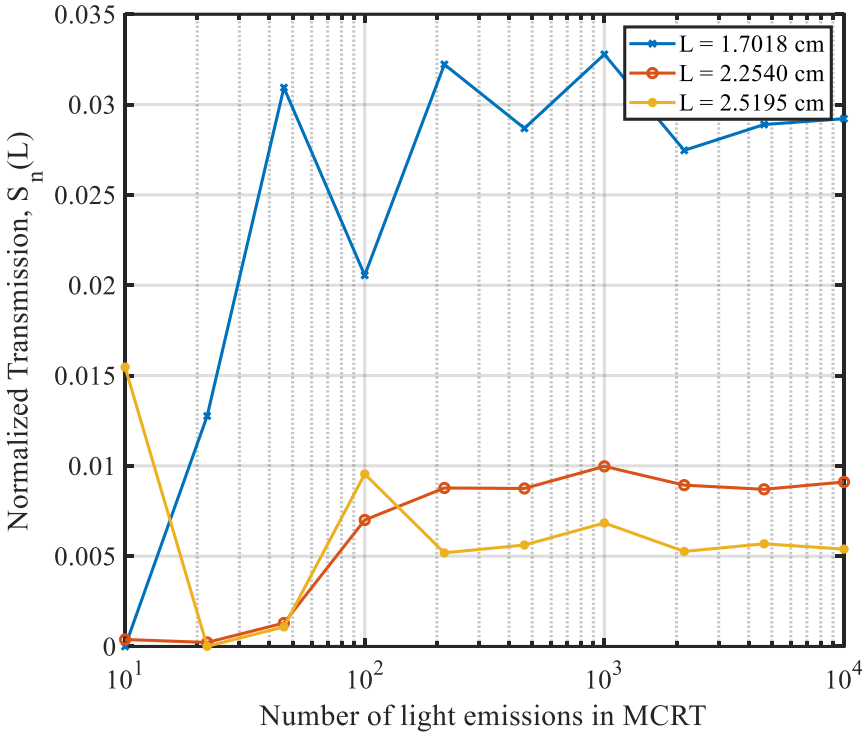

Figure 12 MCRT convergence study

inaccurate material property information in the literature, and additional assumptions of MCRT such as specular surface, temperature, and wavelength independence. The present MCRT simulation is repeated 30 times to obtain uncertainty metrics. The error is more significant at bed heights where negligible transmission can occur. The comparison of overall transmission is essential, since the transmission of a packed bed is directly related to the radiative properties of the structure, such as absorption coefficient, scattering coefficient, and radiative conductivity.

CHAPTER III

GAUSSIAN PROCESS MODEL COUPLED WITH MCRT

This chapter focuses on the method of coupling MCRT model with predictive Gaussian process (GP) to enhance the predictability of radiative properties in the presence of particle size polydispersity. A physical model of porous media used in MCRT simulations is generally built via a Discrete Element Model (DEM) particle settlement simulation. The DEM simulation can provide high fidelity models for various porous structures from dilute to packed media. However, the computational modelling becomes challenging when dealing with large numbers of particles in large-scale MCRT simulations. Machine learning models offer viable approaches to overcome this challenge in computational modelling. A specific porous medium geometry can be described as a probability distribution of lengths travelled by rays in the medium without radiative extinction (i.e. penetration lengths). Gaussian Process model is used to learn the relationship between geometric parameters of porous medium and penetration length probability distribution function. To establish the credibility of study, probability function from the Gaussian process is tested for the absorption calculation of layering powders used in 3D printing. The test results prove that the proposed machine learning model effectively assists MCRT simulations to calculate particulate absorption as a function of geometric, optical, and material properties.

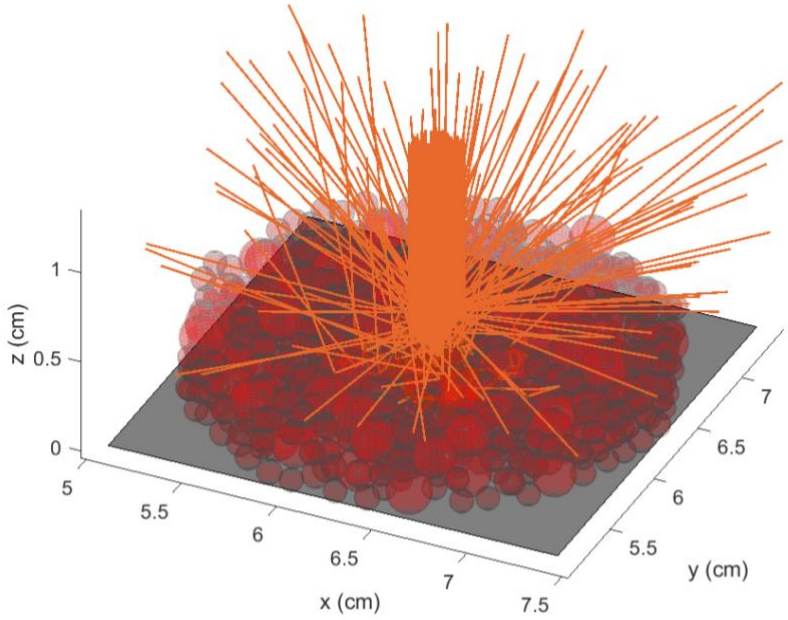

Figure 13 Repeated random sampling of rays emitted to stainless steel powders

3.1 Ray tracing simulation with polarization effect

As mentioned in the previous section, ray tracing can be used to statistically approximate radiative properties such as absorptance which is the ratio of absorbed to the incident radiation. In principle, tracking a sufficient number of random rays traveling in a porous structure can accurately approximate statistical characteristics of the radiative heat transfer process. Figure 13 shows an example of simulated laser rays interacting with stainless steel powder and substrate. Light energy bundles emitted from a certain height

with a specified beam profile are traced iteratively. Each tracing simulation is a loop with the two termination conditions: (1) all the energy in a ray is depleted (absorption) or (2) the ray leaves system (scattering). This conditional tracking loop includes the following operations. At every point, it is determining which particle will next interact with the light ray based on a minimum distance criterion. At each interaction with the solid, a light energy bundle has varying power depending on particle material, radiation wavelength, and incident angle. The power can be calculated by combining the perpendicular (S) and parallel (P) components of the electric fields using the Fresnel equations at the interface of solid-void [3], [4]:

$$\alpha_p(\theta) = 1 - \left| \frac{n^2 cos\,\theta - (n^2 - sin^2\theta)^{1/2}}{n^2 cos\,\theta + (n^2 - sin^2\theta)^{1/2}} \right|^2 \quad (12)$$

$$\alpha_s(\theta) = 1 - \left| \frac{\cos\theta - (n^2 - sin^2\theta)^{1/2}}{\cos\theta + (n^2 - sin^2\theta)^{1/2}} \right|^2 \quad (13)$$

After each interaction, the next direction of light energy bundle is determined assuming specular reflection. If an incident ray hits a substrate, the probability of reflection is calculated and the process is continued in the case of reflection. Absorptance is the ratio of total energy deposited into powder beds to the total emitted energy. There are two main factors to consider vis-à-vis the computational efficiency of ray tracing, namely the computational modelling of powder bed geometry and the simulation of the ray tracing procedure for numerous particles. To overcome these challenges, efficient

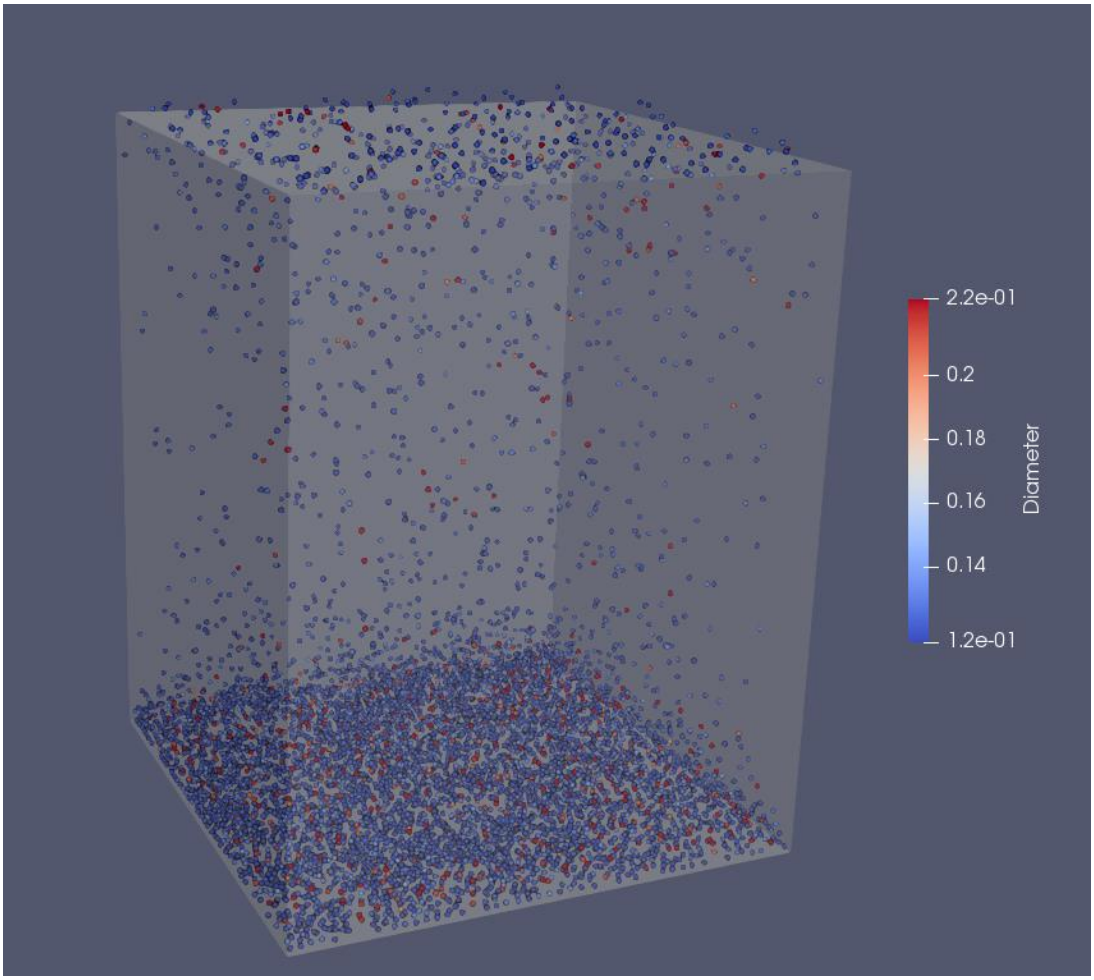

Figure 14 Sequential settling of individual rigid particles in MFIX

abstraction of powder geometry and implementation of abstracted geometry in ray tracing simulations are necessary.

3.2 Computational model of powder geometry

Computational modeling of a porous media structure is essential in ray tracing and subsequent heat radiation analysis. Although a 3D picture of porous media geometry can

be obtained via computed tomography techniques, simulated structures are advantageous in ray tracing because of simple construction and detailed geometric information. In the current work, all geometry models are computationally generated by using an open-source software called MFIX [5]. A discrete element model (DEM) in MFIX simulates the slow sequential settling of individual rigid particles from dilute suspension into a randomly packed assemblage as seen in Figure 14.

Simulations are limited to two-phase flows consisting of dispersed solid particles with varying size and density in a gas phase. The presence of embedded particles in a carrier phase inherits random nature to two-phase flows. Lagrangian-Eulerian (LE) statistical description is implemented for meaningful characterization [6], [7]. In LE representation, a carrier phase is treated as a continuum. A set of conservation equations such as mass and momentum balances is applied for carrier phase modeling. MFIX takes volume and ensemble statistical averaging approaches to obtain the continuum conservation equations [8]–[10]. Conversely, the dispersed phase is treated as being made of discrete entities. Each distinct solid phase is characterized by a unique particle size distribution. In actual simulations, the solid phase is represented by actual individual particles and the collisions are directly resolved using the soft-sphere based on a spring-dashpot model [11].

In the overall workflow of MFIX, DEM solutions are coupled with a computational fluid dynamics (CFD) solver to solve granular flows in continuum fluid. Once the coupling is enabled, at a certain CFD time step, the conservation equations are solved iteratively by the CFD solver, and the calculated drag forces and fluid-solid

momentum transfer are passed to the DEM solvers. Then, multiple DEM time steps are carried out to integrate the equations of motion associated with the particles for the given contact and drag forces.

Additionally, advanced development is available in MFIX to enable particle-size polydispersity [12]. Newly added arrays assign each solid particle a unique phase index depending on its diameter, which helps in phase-specific physical properties of the particles to be retrieved and employed in the subsequent computation of particle contact forces. These properties include material density, Young's modulus, coefficient of friction, and coefficient of restitution. In particular, arrays with a size of the total particle number save the diameter of each particle in the system. The phase index of each particle is assigned based on its physical properties instead of its diameter. The change of data structure for saving and retrieving an individual particle diameter affects a number of subroutines which utilize the array as input for subsequent calculations. The subroutines include particle force/torque calculation, solid–gas momentum transfer calculation, grid cell locator and neighbor locator. Size distribution of the solid phase can be assigned for both initial condition and mass-in-flow boundary conditions. By specifying this information, the simulation of complex multiphase flow can be processed during which additional solids are injected into the system.

The end result of these assignments and procedures are the locations and sizes of numerous particles. Ray tracing simulations use this information to perform heat analysis. With a large and complex geometry background, the computational load increases as polynomial function of system configuration size. Therefore, the probability distribution

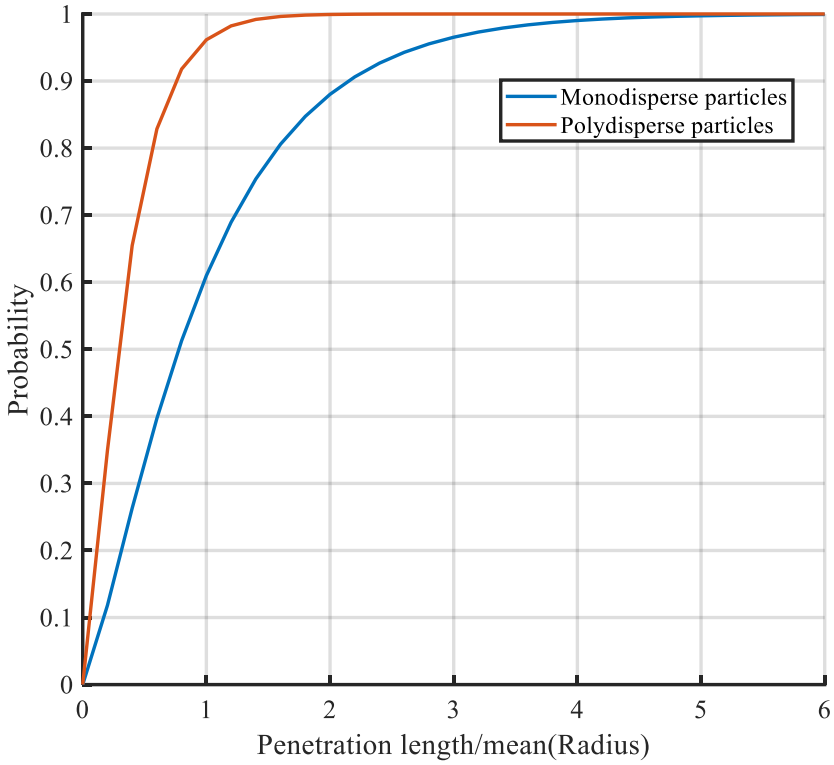

Figure 15 Penetration length probability density function

of penetration length (the distribution of probable extinction-free paths between solid elements) is used to abstract out and summarize the geometric information. This distribution is closely related to the radiative properties of a particulate geometry [13]. Any porous media geometry can be expressed by this probabilistic model regardless of size and complexity. The ray tracing simulation calculates how far rays emitted from randomly selected particles can travel in porous media without experiencing extinction. The particles which have six contacts to adjacent particles are only picked for meaningful

statistical results. Figure 15 shows two penetration length probability density functions for powder models with monodisperse and polydisperse particles.

3.3 Machine learning based geometry abstraction

Computing penetration length probability density functions entail complex geometry modelling and ray tracing. Machine learning models can be used to learn how a probability distribution function of penetration length changes as a function of geometric parameters. The objective of this implementation is to test the feasibility of machine learning in mapping the large-scale Cartesian based geometry data to simple distribution functions of the penetration length. Once successfully learned, the models can generate the probability functions without demanding heavy computations. Considering high complexity in the mapping between powder geometry and a desired probability functions, Gaussian Process (GP) is a suitable choice for geometry abstraction.

The GP training characterizes basis function coefficients, β, the noise variance, σ^2, and the kernel parameter, θ. The GP regression model is equivalent to

$$P(y|f,X) \sim N(y|H\beta + f, \sigma^2 I)$$

$$X = \begin{pmatrix} x_1^T \\ x_2^T \\ \vdots \\ x_n^T \end{pmatrix}, Y = \begin{pmatrix} y_1 \\ y_2 \\ \vdots \\ y_n \end{pmatrix}, H = \begin{pmatrix} h(x_1^T) \\ h(x_2^T) \\ \vdots \\ h(x_n^T) \end{pmatrix}, Y = \begin{pmatrix} f(x_1) \\ f(x_2) \\ \vdots \\ f(x_n) \end{pmatrix} \quad (14)$$

The joint distribution of latent variables in GP regression model is as follows:

$$P(f|X) \sim N(f|0, K(X,X)) \quad (15)$$

where $K(X,X)$ is the matrix of covariance function$k(x,x')$. $k(x,x')$ is parameterized by θ. Input sets are made of two size distribution parameters and percentile of penetration length.

$$x = \begin{pmatrix} {R_{mean}}^T \\ {R_{STD}}^T \\ p^T \end{pmatrix}, y = l \quad (16)$$

3.4 Modified ray tracing

In order to efficiently utilize probabilistic models obtained from Gaussian Process, the ray tracing model must be modified algorithmically [4], [40]. The proposed model still focuses on absorption calculation based on statistical sufficient ray tracing. However, the memory of particle coordinates is no longer required to trace a ray. Instead, random angles and penetration length distribution are used to create probable paths of rays in a specific powder geometry. This change transforms the form of randomness from random sphere packing to random trajectories of traveling light. In simulation, the random packed bed structure is gradually constructed as a light bundle travels through the bed using penetration length distribution. The light bundle transmits through vacuum void in the bed and experiences absorption and scattering due to particles. These simultaneous processes of structure formation and ray tracing reduce computation cost significantly.

An iteration loop in modified ray tracing starts with emitting a light bundle downwards from a certain height. The first interaction with solid phase occurs at a

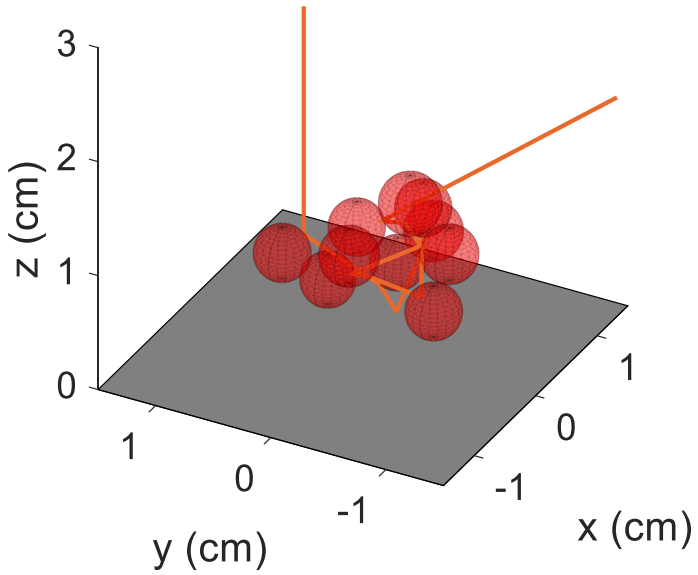

Figure 16 Modified ray tracing simulation

predetermined powder bed height. From the interaction point, a center coordinates of interacting particle is chosen randomly as explained before in section 2.3. The attenuation of light bundle energy at the interaction point is calculated with Fresnel equations instead of using gray surface assumption. By adapting the Fresnel equations, the simulation model can account for the angular and polarization dependency of the absorption of incident rays. After the energy attenuation calculation, the specularly reflected light bundle heads to the next interaction point. The direction of this reflected ray is calculated as the same, but the magnitude is randomly assigned from the penetration length probability function generated by GP model. The stop conditions for a iteration loop is same as those described

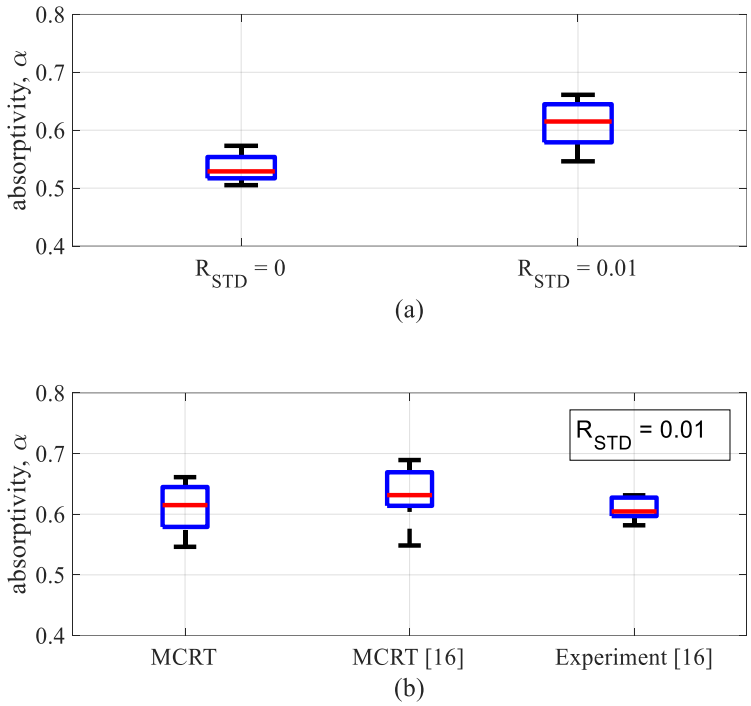

Figure 17 (a) Absorptivity comparison (b) Ray tracing performance

in section 2.3, but the first scatter back condition is no longer applicable due to a substrate at the bottom boundary. Any radiation ray that hits the substrate is specularly reflected with attenuated radiation energy and the iteration loop continues until one of the two conditions met. The normalized absorptivity is approximated by dividing the total energy of bundles accumulated to solid phase, by the total energy of light bundles emitted in the bed. Figure 16 shows a sample run of modified ray tracing simulation.

3.5 Results and discussion

The performance of ray tracing is evaluated by comparing results with those of the literature. Figure 17(a) shows total absorptivity of monodisperse and polydisperse powder bed, calculated from the ray tracing without the modifications. Materials for both powder models are stainless steel. Thus, the gap between two absorptivity values is derived from geometric distinction between the two models. The last two values in Figure 17(b) represent absorptivities of polydisperse powder model determined from a literature study [41]. These two numerical and experimental results confirm the validity of the proposed ray tracing model. After sufficient penetration lengths are obtained from two powder models, the averages of two penetration sets are calculated, which are 0.716cm and 0.747cm for monodisperse and polydisperse particles, respectively. These results indicate that rays are more likely to experience more scattering within polydispersity particles. Due to increased light trapping, higher absorptivity is observed for polydisperse particles as seen in Figure 17(a).

A GP model is trained to predict a penetration length probability function given a geometric input set. Figure 18 shows the comparison between true response and predicted response. To measure the improbability of a curve fit in GP model, regression loss on the training data is computed. The type of regression loss used here is re-substitution loss. The loss output, L = 0.0055, demonstrates that the fit is good and only few outliers exist. Thus, the use of this GP model is justifiable.

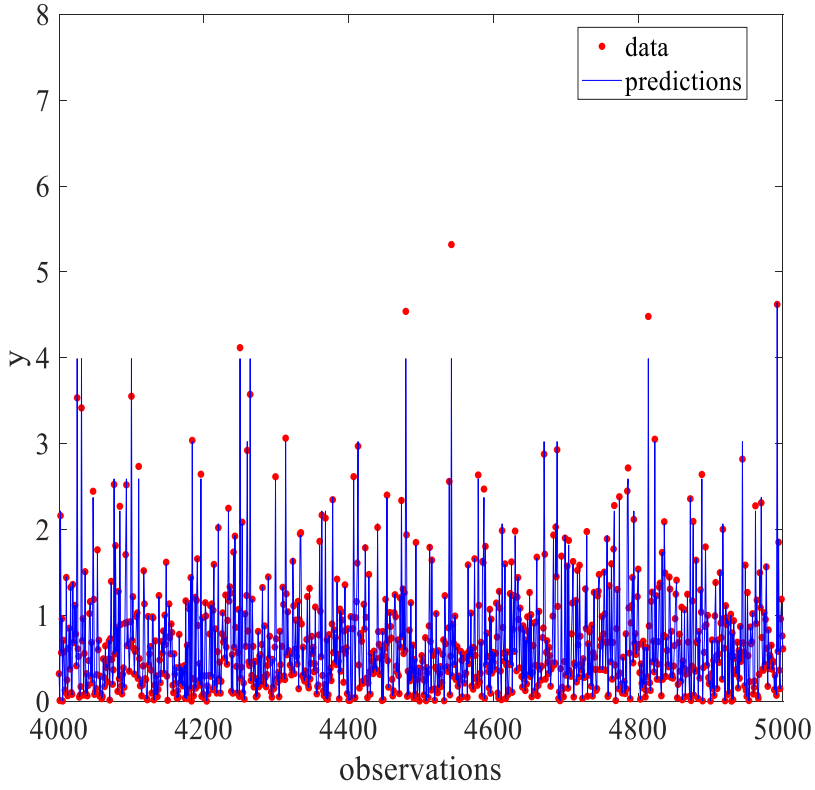

Figure 18 Performance of trained GP model

The trained GP model is coupled with the modified ray tracing to generate random penetration lengths. Then, the performance of the modified ray tracing model is analysed by comparing results with the original ray tracing and the literature. Table 2 lists six materials popularly used in AM industry. Each material has distinct optical properties. Along with material information, Table 2 shows absorptivity of each material, calculated by the two ray tracing methods. The two absorptivity output sets agree well with each other. In addition, no significant deviations exist between modified ray tracing output and the literature values. Consequently, the GP model is successfully applied and preserves the computational accuracy. To evaluate the efficiency of the proposed modified ray

tracing approach, CPU times of the two models are computed and compared. Both simulations have the same settings so that the difference in results can only be attributed to algorithms discrepancies. Specifically, ZnO is used as the layering material and 5000 rays are emitted. The resulting CPU times for original ray tracing and modified ray tracing model are 9.72 sec. and 276.66 sec., respectively. One possible reason the modified model takes more time than the original model is the iterative neighbour searches required for the impenetration constraint. However, if the computation cost of geometry modelling is considered, the modified ray tracing approach is significantly more efficient that the conventional models. Specifically, the CPU time for computational modelling of polydisperse powder model was 2.526 days. This exhaustive cost was avoided by using geometric GP model.

Table 2 Absorptivity calculations of AM materials (modified from [2] & [7])

Material	Refractive index (n)		Absorptivity (α)		
	Re	Im	Ray tracing	Modified	Literature [2], [7]
Cu	0.35	6.97	0.13	0.14	0.17
SS	3.27	4.48	0.62	0.6	0.6
Ag	0.23	7.09	0.12	0.12	0.13
PMMA	1.4831	57.4	0.02	0.03	0.06
Al_2O_3	1.7579	0	0.969	0.95	0.96
ZnO	1.998	0	0.953	0.93	0.94

CHAPTER IV

CONCLUSION

A NN model was developed for the purpose of predicting radiative transmission through randomly packed beds. The MCRT simulation was used a limited number of times to collect training data required for the NN regression. During training, the link weights are adjusted iteratively so that the overall error of the network is minimized for each training example. The performance of trained NN model was measured in terms of regularized sum of squared errors. The regularized sum of squared errors were minimized to 0.005 and 0.0025 for validation and training error, respectively. The results of NN-based transmission prediction made a good agreement with the results from previously measured literature results. Depending on the geometry of packed bed, the CPU time required for a MCRT simulation ranges from 5 to 20 minutes. Meanwhile, with training, the NN model took around 10 seconds in average to calculate transmittivity. All CPU time calculations do not include the cost of the computational modelling of packed bed geometry. However, the cost of packed bed modelling is significant in terms of computational efficiency. Thus, as a second purpose of ML implementation, a GP model was developed to abstract each complex particulate geometry into a particular probability function of penetration length. The coupling of GP model with ray tracing enabled accurate and efficient prediction of six AM powder absorptivity calculations. A ray tracing algorithm was modified to achieve efficient coupling. The calculation errors between original ray tracing and coupled ray tracing model ranged from 1.96% to 7.69% and the

errors between coupled ray tracing and literature results ranged from 1.05% to 21.4%. With the same input setting, the CPU time for a ray tracing calculation increased by 27.5% after coupling. However, the coupled ray tracing model is still more efficient than the original ray tracing model if the cost of packed bed geometry modelling is considered.

REFERENCES

[1] J. R. Howell, M. P. Menguc, and R. Siegel, *Thermal radiation heat transfer*. CRC Press, 2010.

[2] C. D. Boley, S. A. Khairallah, and A. M. Rubenchik, "Calculation of laser absorption by metal powders in additive manufacturing," *Appl. Opt.*, vol. 54, no. 9, p. 2477, Mar. 2015.

[3] A. V. Gusarov and J.-P. Kruth, "Modelling of radiation transfer in metallic powders at laser treatment," *Int. J. Heat Mass Transf.*, vol. 48, no. 16, pp. 3423–3434, Jul. 2005.

[4] Y. S. Yang, J. R. Howell, and D. E. Klein, "Radiative heat transfer through a randomly packed bed of spheres by the Monte Carlo method.," *Am. Soc. Mech. Eng.*, vol. 1, no. May 1983, 1982.

[5] J. C. Chen and S. W. Churchill, "Radiant heat transfer in packed beds," *AIChE J.*, vol. 9, no. 1, pp. 35–41, Jan. 1963.

[6] R. J. Cimini and J. C. Chen, "Experimental measurements of radiant transmission through packed and fluidized media," *Exp. Heat Transf.*, vol. 1, no. 1, pp. 45–56, Jan. 1987.

[7] N. K. Tolochko, Y. V. Khlopkov, S. E. Mozzharov, M. B. Ignatiev, T. Laoui, and V. I. Titov, "Absorptance of powder materials suitable for laser sintering," *Rapid Prototyp. J.*, vol. 6, no. 3, pp. 155–161, Sep. 2000.

[8] "RDFI determination of anisotropic and scattering dependent radiative conductivity tensors in porous media: Application to rod bundles," *Int. J. Heat Mass Transf.*, vol. 52, no. 5–6, pp. 1544–1551, Feb. 2009.

[9] D. Moser, S. Pannala, and J. Murthy, "Computation of effective radiative properties of powders for selective laser sintering simulations," *JOM*, vol. 67, no. 5, pp. 1194–1202, May 2015.

[10] C. Argento and D. Bouvard, "A ray tracing method for evaluating the radiative heat transfer in porous media," *Int. J. Heat Mass Transf.*, vol. 39, no. 15, pp. 3175–3180, Oct. 1996.

[11] G. E. Imoberdorf, O. M. Alfano, A. E. Cassano, and H. A. Irazoqui, "Monte Carlo model of UV-radiation interaction with TiO2-coated spheres," *AIChE J.*, vol. 53, no. 10, pp. 2688–2703, Oct. 2007.

[12] B. P. Singh and M. Kaviany, "Independent theory versus direct simulation of

radiation heat transfer in packed beds," *Int. J. Heat Mass Transf.*, vol. 34, no. 11, pp. 2869–2882, 1991.

[13] B. X. Wang and C. Y. Zhao, "Modeling radiative properties of air plasma sprayed thermal barrier coatings in the dependent scattering regime," *Int. J. Heat Mass Transf.*, vol. 89, pp. 920–928, Oct. 2015.

[14] X. C. Wang, T. Laoui, J. Bonse, J. P. Kruth, B. Lauwers, and L. Froyen, "Direct selective laser sintering of hard metal powders: experimental study and simulation," *Int. J. Adv. Manuf. Technol.*, vol. 19, no. 5, pp. 351–357, Mar. 2002.

[15] W. S. Jodrey and E. M. Tory, "Simulation of random packing of spheres," *Simulation*, vol. 32, no. 1, pp. 1–12, Jan. 1979.

[16] S. Chen, M. Adepu, H. Emady, Y. Jiao, and A. Gel, "Enhancing the physical modeling capability of open-source MFIX-DEM software for handling particle size polydispersity: Implementation and validation," *Powder Technol.*, vol. 317, pp. 117–125, Jul. 2017.

[17] M. Tancrez and J. Taine, "Direct identification of absorption and scattering coefficients and phase function of a porous medium by a Monte Carlo technique," *Int. J. Heat Mass Transf.*, vol. 47, no. 2, pp. 373–383, 2004.

[18] J. Taine and E. Iacona, "Upscaling statistical methodology for radiative transfer in porous media: new trends," *J. Heat Transfer*, vol. 134, no. 3, p. 031012, Mar. 2012.

[19] S. Haussener, W. Lipiński, J. Petrasch, P. Wyss, and A. Steinfeld, "Tomographic characterization of a semitransparent-particle packed bed and determination of its thermal radiative properties," *J. Heat Transfer*, vol. 131, no. 7, 2009.

[20] S. Haussener, P. Coray, W. Lipiński, P. Wyss, and A. Steinfeld, "Tomography-based heat and mass transfer characterization of reticulate porous ceramics for high-temperature processing," *J. Heat Transfer*, vol. 132, no. 2, p. 023305, Feb. 2010.

[21] P. Parthasarathy, P. Habisreuther, and N. Zarzalis, "Identification of radiative properties of reticulated ceramic porous inert media using ray tracing technique," *J. Quant. Spectrosc. Radiat. Transf.*, vol. 113, no. 15, pp. 1961–1969, 2012.

[22] M. Chahlafi, F. Bellet, F. Fichot, and J. Taine, "Radiative transfer within non Beerian porous media with semitransparent and opaque phases in non equilibrium: Application to reflooding of a nuclear reactor," *Int. J. Heat Mass Transf.*, vol. 55, no. 13–14, pp. 3666–3676, Jun. 2012.

[23] J. Randrianalisoa and D. Baillis, "Analytical model of radiative properties of packed beds and dispersed media," *Int. J. Heat Mass Transf.*, vol. 70, pp. 264–275, Mar.

2014.

[24] L. A. Dombrovsky and D. Baillis, *Thermal radiation in disperse systems: an engineering approach*. Begellhouse, 2010.

[25] D. Baillis and J.-F. Sacadura, "Thermal radiation properties of dispersed media: theoretical prediction and experimental characterization," *J. Quant. Spectrosc. Radiat. Transf.*, vol. 67, pp. 327–363, 2000.

[26] N. Metropolis and S. Ulam, "The Monte Carlo method," *J. Am. Stat. Assoc.*, vol. 44, no. 247, pp. 335–341, Sep. 1949.

[27] C. E. Rasmussen and C. K. I. Williams, *Gaussian processes for machine learning*. MIT Press, 2006.

[28] Y. S. Yang, J. R. Howell, and D. E. Klein, "Radiative heat transfer through a randomly packed bed of spheres by the Monte Carlo method.," *Am. Soc. Mech. Eng.*, vol. 1, no. May 1983, 1982.

[29] J. R. Howell, M. P. Menguc, R. Siegel, M. P. Menguc, and R. Siegel, *Thermal radiation heat transfer, 6th edition*. CRC Press, 2015.

[30] M. Q. Brewster and C. Tien, "Radiative transfer in packed fluidized beds: dependent versus independent scattering," *J. Heat Transfer*, vol. 104, no. November 1982, pp. 573–579, 1982.

[31] M. T. Hagan, H. B. Demuth, M. H. Beale, and O. De Jesus, *Neural network design*. Campus Pub. Service, University of Colorado Bookstore, 2014.

[32] A. H. Aly and R. C. Peralta, "Optimal design of aquifer cleanup systems under uncertainty using a neural network and a genetic algorithm," *Water Resour. Res.*, vol. 35, no. 8, pp. 2523–2532, 1999.

[33] F. D. Foresee and M. T. Hagan, "Gauss-Newton approximation to Bayesian regularization," in *Proceedings of the 1997 International Joint Conference on Neural Networks*, 1997, pp. 1930–1935.

[34] D. J. C. MacKay, "A practical bayesian framework for backpropagation networks," *Neural Comput.*, vol. 4, no. 3, pp. 448–472, 1992.

[35] N. V. Queipo, R. T. Haftka, W. Shyy, T. Goel, R. Vaidyanathan, and P. Kevin Tucker, "Surrogate-based analysis and optimization," *Prog. Aerosp. Sci.*, vol. 41, no. 1, pp. 1–28, 2005.

[36] A. Krogh, J.Vedelsby, "Neural network ensembles, cross validation, and active learning, " *Advances in neural information processing systems*, pp. 231-238, 1995.

[37] F. A. C. Viana, R. T. Haftka, and L. T. Watson, “Efficient global optimization algorithm assisted by multiple surrogate techniques,” *J. Glob. Optim.*, vol. 56, no. 2, pp. 669–689, 2013.

[38] A. Clauset, C. R. Shalizi, and M. E. J. Newman, “Power-law distributions in empirical data,” *SIAM Review*, 51(4), 661-703, Jun. 2007.

[39] John C. Chen and S. W. Churchill, “Radiant heat transfer in packed beds,” *AIChE J.*, vol. 9, no. 1, pp. 35–41, 1963.

[40] H. H. Kang, M. Kaya, and S. Hajimirza, “A data driven artificial neural network model for predicting radiative properties of metallic packed beds,” *J. Quant. Spectrosc. Radiat. Transf.*, vol. 226, pp. 66–72, Mar. 2019.

[41] W. King, A. T. Anderson, R. M. Ferencz, N. E. Hodge, C. Kamath, and S. A. Khairallah, “Overview of modelling and simulation of metal powder bed fusion process at Lawrence Livermore National Laboratory,” *Mater. Sci. Technol.*, vol. 31, no. 8, pp. 957–968, Jun. 2015.